

# Increased mitochondrial nanotunneling activity, induced by calcium imbalance, affects intermitochondrial matrix exchanges

Manuela Lavorato<sup>1</sup>, V. Ramesh Iyer<sup>2</sup>, Williams Dewight<sup>3</sup>, Ryan Cupo<sup>4</sup>, Valentina Debattisti<sup>4</sup>, Ludovic Gomez<sup>5</sup>, Sergio De la Fuente<sup>4</sup>, Yan-Ting Zhao<sup>6</sup>, Héctor H. Valdivia<sup>6</sup>, György Hajnóczky<sup>4</sup>, Clara Franzini-Armstrong<sup>1</sup>

<sup>1</sup>Dept. of Cell Developmental Biology, U. of Pennsylvania, Philadelphia; <sup>2</sup>Division of Cardiology, Children's Hospital of Philadelphia; <sup>3</sup>Biomedical Research Core Facility, U. of Pennsylvania, Philadelphia; <sup>4</sup>MitoCare Center Dept. of Pathology, Anatomy and Cell Biology, Thomas Jefferson University, Philadelphia; <sup>5</sup>Dept. of Medicine, Center for Translational Medicine, Thomas Jefferson University, Philadelphia; <sup>6</sup>Dept. of Internal Medicine, U. of Michigan.

Submitted to Proceedings of the National Academy of Sciences of the United States of America

**Exchanges of matrix contents are essential to the maintenance of mitochondria. Cardiac mitochondria exchange matrix content in two ways: by direct contact with neighboring mitochondria and over longer distances. The latter mode is supported by thin tubular protrusions, called nanotunnels that contact other mitochondria at relatively long distances. Here, we report that cardiac myocytes of heterozygous mice carrying a Catecholaminergic Polymorphic Ventricular Tachycardia (CPVT) – linked RyR2 mutation (A4860G) (Zhao Y-T, et al. (2015) Proc Natl Acad Sci USA 112: 1669-1677) show unique and unusual mitochondria response: a significantly increased frequency of nanotunnel extensions. The mutation induces Ca<sup>2+</sup> imbalance by depressing RyR2 channel activity during excitation – contraction (E-C) coupling and resulting in random bursts of Ca<sup>2+</sup> release probably due to Ca<sup>2+</sup> overload in the sarcoplasmic reticulum. We took advantage of the increased nanotunnels frequency in RyR2<sup>A4860G/+</sup> cardiomyocytes to investigate and accurately define the ultrastructure of these mitochondria extensions and to reconstruct the overall 3D distribution of nanotunnels using electron tomography. Additionally, in order to define the effects of communication via nanotunnels, we evaluated the intermitochondrial exchanges of matrix-targeted soluble fluorescent proteins, mtDsRed and photoactivable mtPA-GFP, in isolated cardiomyocytes by confocal microscopy. A direct comparison between exchanges occurring at short and long distances, directly demonstrates that communication via nanotunnels is slower.**

Mitochondria | nanotunnels | CPVT | RyR2 | mitochondria dynamics

## Introduction

Recent concepts of mitochondrial structure and function oscillate between two divergent views. One view emphasizes the totally dynamic concept of a mitochondrial system, as seen in bacteria and cultured cells, represented by individual elements that enjoy extensive mobility combining large migrations between different areas of the cells with dynamic tubulation, fusion and fission processes (1-3). At the opposite end of the spectrum is a restricted static view of mitochondria, as seen in mouse skeletal muscle, in which mitochondria constitute a semi-permanent extensive network that allows intracellular energy distribution (4). Obviously, neither extreme view applies perfectly to all cells, tissues and functional conditions. In differentiated skeletal and cardiac muscle, mitochondria are stabilized in a stereotyped positioning relative to myofibrils mostly because their movements are restricted by the narrow spaces between the myofibrils and also because they are specifically tethered, perhaps via mitofusin-2 to the membrane systems, mostly the sarcoplasmic reticulum (SR) (5-8). Exchange of matrix content, DNA and proteins and segregation of damaged mitochondrial components are needed for maintaining mitochondria and cell functions (9, 10). Striated muscles have developed a unique system of inter mitochondrial communication either directly at short distances or via long nanotunnel extensions

(11, 12). Neither type of communication apparently requires a migration of the organelles from their tethered sites. Unique intimate contacts, “kissing junctions”, coordinate structural associations between mitochondria (13).

Ca<sup>2+</sup> plays two major roles in mitochondrial functions. One is to regulate oxidative energy production, permeability transition and other processes in the mitochondrial matrix (14). The other one is to control mitochondrial dynamics via fission by targeting of Drp1 (15, 16) and via motility by targeting Miro proteins (17-19) in the cytoplasm. In some striated muscles, including mammalian myocardium, mitochondria are strategically located for uptake and sensing of small amount of Ca<sup>2+</sup> during its release from the adjoining SR (6, 20, 21). This makes mitochondria particularly responsive to changes in Ca<sup>2+</sup> homeostasis. Cardiac ryanodine receptor (RyR2) is the SR Ca<sup>2+</sup> release channel involved in normal excitation-contraction E-C coupling in cardiac muscle. Mutations in skeletal ryanodine receptor (RyR1) resulting in unbalanced Ca<sup>2+</sup> homeostasis can affect mitochondria morphology and distribution (22, 23). Defects in mitochondrial dynamics and mitochondrial morphology have also been reported in various cardiomyopathies and heart failure but have not been linked to Ca<sup>2+</sup> homeostasis.

In this communication we demonstrate an unusual cardiac mitochondrial response to an engineered RyR2 mutation

## Significance

Nanotunnels are long thin mitochondrial extensions that have been implied in direct long distance (1 to >5 μm) communication between mitochondria of cardiac myocytes. The engineered RyR2<sup>A4860G/+</sup> mutation, resulting in loss of function of the Sarcoplasmic Reticulum calcium release channel and arrhythmia, induces a striking increase in the frequency of long distance intermitochondrial communication via nanotunnels without involvement of obvious mitochondria migration. We use this model for exploring the significance of mitochondria nanotunneling in myocardium and the contribution of microtubules to the formation of these unusual organelle extensions using EM tomography and live confocal imaging. This study constitutes an approach to arrhythmia investigations that focuses on a new target: the mitochondria.

## Reserved for Publication Footnotes

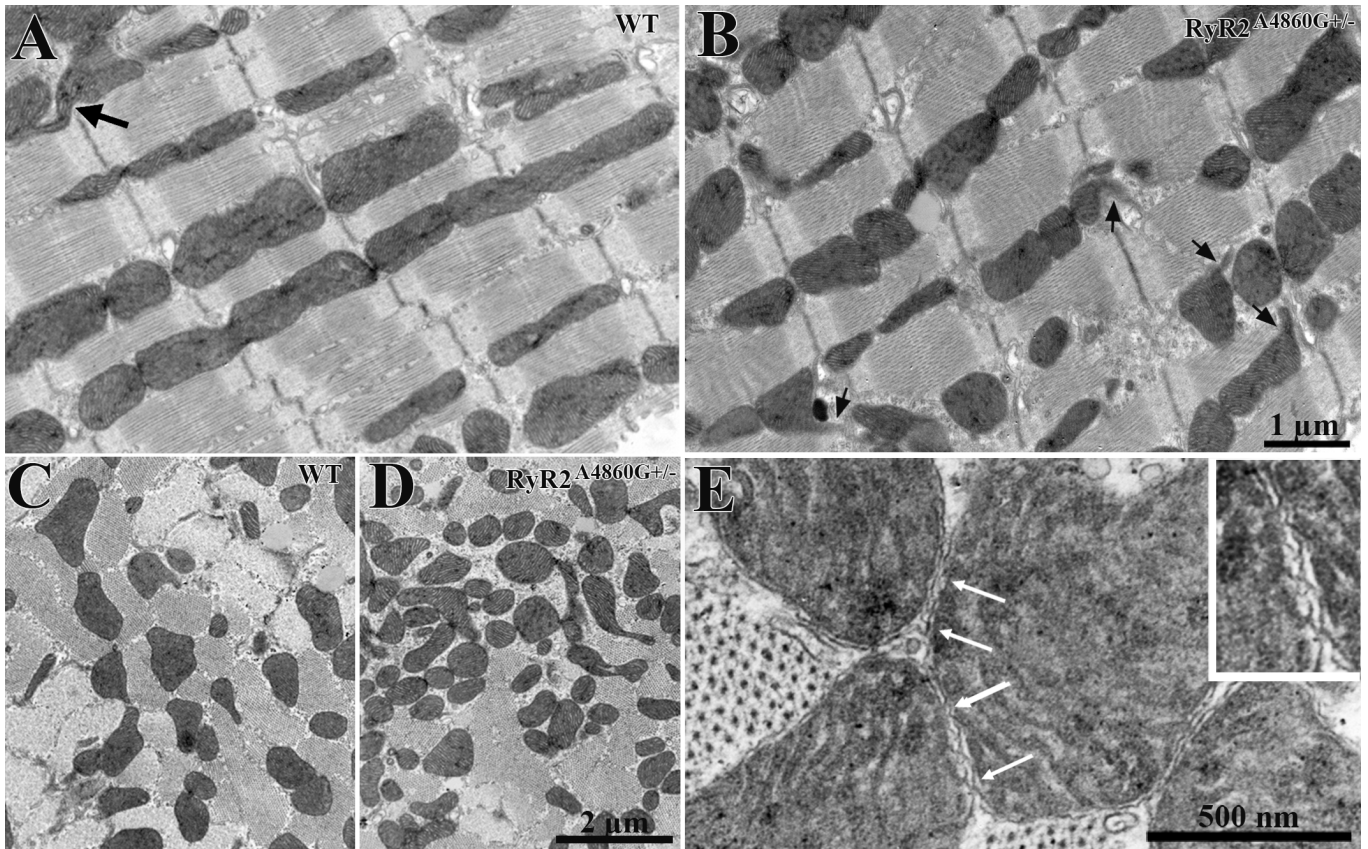


**Fig. 1. Mitochondria in WT and  $RyR2^{A4860G\pm}$  cardiomyocytes.** A, B) Thin longitudinal sections of WT and  $RyR2^{A4860G\pm}$  myocytes. Mitochondria are longitudinally arranged in the spaces between the myofibrils, often in single file, constituting  $\sim 40\%$  of the cell volume. The majority of mitochondria are cylindrical in shape with a variable diameter and length. Larger mitochondria infrequently extend protrusions called "nanotunnels" (arrows), which are less frequent in WT (A) than in  $RyR2^{A4860G\pm}$  (B). C, D) In cross sections the intersections of mitochondria and nanotunnels with the plane of section constitute separate profiles, with variable diameter and distribution. Small profiles are less frequent in WT (C) than  $RyR2^{A4860G\pm}$  (D). E) Contiguous mitochondria form "kissing junctions" (arrows) at their sites of close proximity. In these specialized contact areas, the outer membrane protrudes into periodic contacts and occasionally the inner membrane participates in the junction. The inset is enlarged by three fold. The frequency of kissing junctions relative to the closely apposed sets of mitochondria does not significantly differ in the two sets of myocytes:  $82\% \pm 19$  in WT and  $89\% \pm 12$  in mutants (mean  $\pm$  SD, 293 mitochondria couples, 30 cardiomyocytes, 3 hearts) (385 mitochondria couples, 32 cardiomyocytes, 3 hearts).

(A4860G). The mutation depresses  $RyR2$  channel activity during E-C coupling, but also results in random bursts of  $Ca^{2+}$  release during systole. Therefore the myocytes are affected by a specific  $Ca^{2+}$  metabolism imbalance, resulting in a form of Catecholaminergic Polymorphic Ventricular Tachycardia (CPVT) (24). The unique mitochondrial response is a striking increase in long distance intermitochondrial communications by widespread nanotunnel extensions (12). The study of  $RyR2^{A4860G\pm}$  cardiomyocytes allows us to define and differentiate between two modes of intermitochondrial communications (close proximity "kissing" and long distance "nanotunneling"), neither of which requires physical migration of the organelles.

## Results

### Ultrastructure of WT and $RyR2^{A4860G\pm}$ cardiomyocytes: variability in mitochondria shapes/disposition

The  $RyR2^{A4860G\pm}$  mutation induces an unexpected, unique mitochondrial response in the myocardium, but does not affect any other structural components (Figs. 1A and 1B). Cardiac mitochondria in WT mice are discrete organelles aligned in either single or multiple longitudinal rows between myofibrils (Fig. 1A). They are approximately cylindrical with rounded edges and occasional short tubular extensions, or nanotunnels (Fig. 1A) (12) and they are longitudinally oriented. The overall appearance and disposition of sectioned mitochondria profiles in myocytes from

the heterozygotes are essentially the same as in WT but with two exceptions. First, the frequency of nanotunnel extensions is noticeably increased and that results in overall distortions of the mitochondrial profiles (Figs. 1B and 2A, D). Secondly, this is accompanied by a visibly higher occurrence of small mitochondrial profiles in mutant (Fig. 1D) vs WT (Fig. 1C) detected in cross sections.

Neighboring mitochondria may join each other either at their ends or laterally at "kissing" junctions, which are very intimate contacts involving a specific narrow proximity of the outer membranes over small spots at short intervals (Fig. 1E) (12, 13). The frequency of kissing junctions, or sites of possible communication between large mitochondria is essentially unaltered in the mutant vs WT. On the average,  $82\%$  in WT and  $89\%$  in mutants of the mitochondria proximity sites have kissing junctions (Fig. 1E).

### Analysis of nanotunnel structure, disposition and frequency

The higher frequency of nanotunnels associated with  $RyR2^{A4860G\pm}$  mitochondria offers the opportunity for an in depth analysis of nanotunnels microanatomy. Nanotunnels are funnel shaped extensions at their origin, their diameters decrease in proximity of the mitochondria and then remain fairly constant within a range of  $0.04 - 0.20 \mu m$  (Fig. 2 A-C). All nanotunnels, even the narrowest ones, clearly have outer and inner membranes; they contain matrix proteins and show a continuation of the cristae, mostly aligned parallel to



273  
274  
275  
276  
277  
278  
279  
280  
281  
282  
283  
284  
285  
286  
287  
288  
289  
290  
291  
292  
293  
294  
295  
296  
297  
298  
299  
300  
301  
302  
303  
304  
305  
306  
307  
308  
309  
310  
311  
312  
313  
314  
315  
316  
317  
318  
319  
320  
321  
322  
323  
324  
325  
326  
327  
328  
329  
330  
331  
332  
333  
334  
335  
336  
337  
338  
339  
340

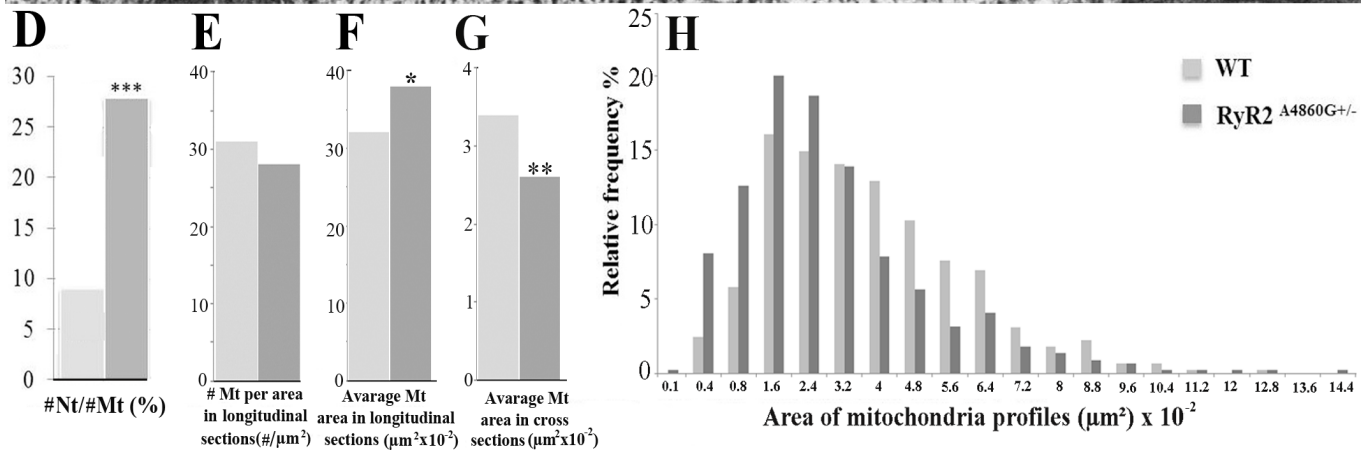
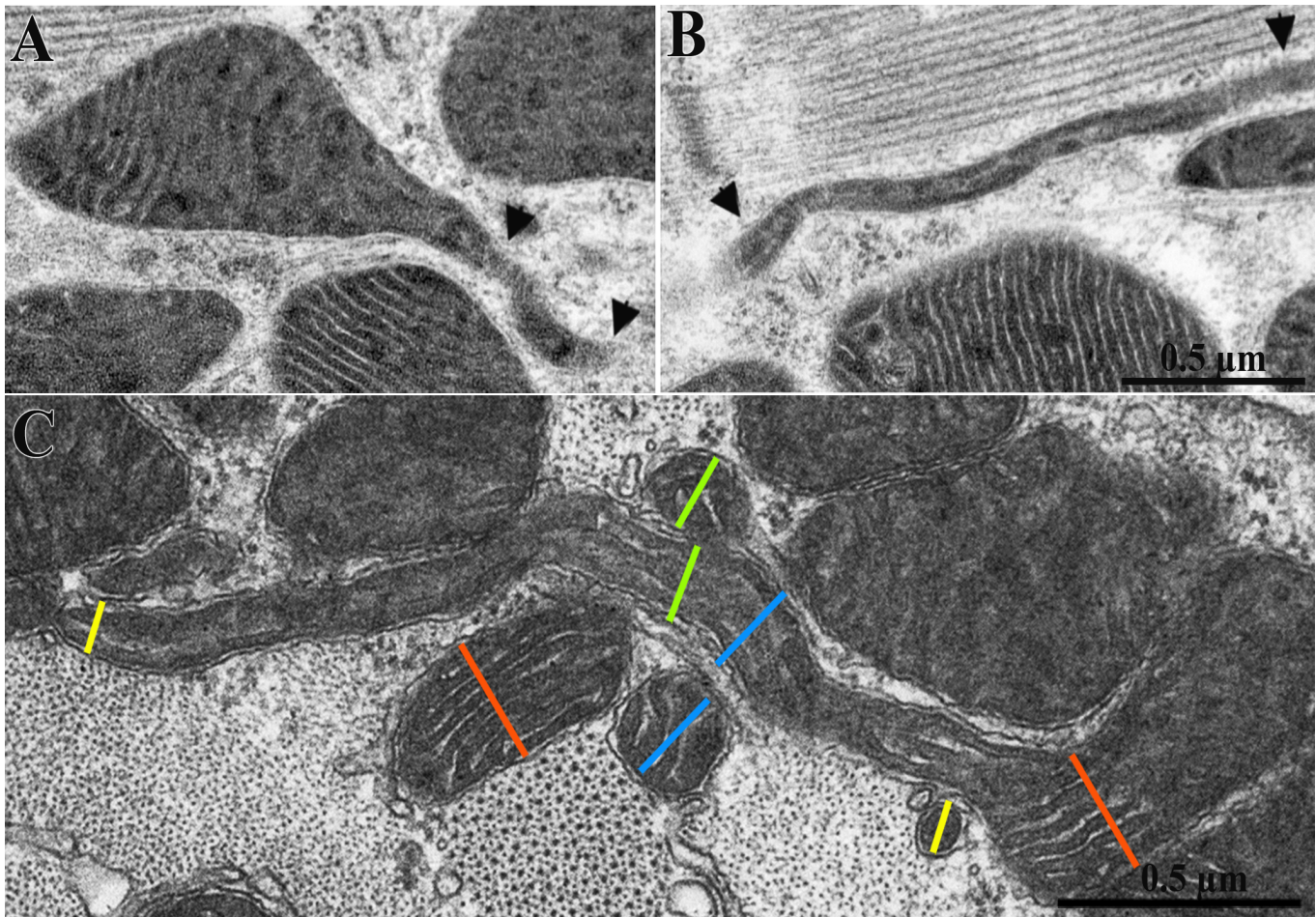


**Fig. 2. Images and quantitation of mitochondria and nanotunnels.** A-C) Mitochondria and nanotunnels in RyR2<sup>A4860G</sup> myocytes. A) Mitochondria's outlines are distorted into a conical protrusion at the site of nanotunnel origin. A short segment of the nanotunnel (between arrowheads) is contained within the section. B) A very thin longitudinally oriented nanotunnel (between arrowheads) is followed for over 2 μm. C) A nanotunnel extends transversely across the fiber from the mitochondrion at right to the one at far left, overpassing and possibly kissing other mitochondria. The cristae are present and aligned parallel to the long axis of the tunnel. Colored lines indicate correspondence between the diameter of a mitochondrion/nanotunnel and the nearby sectioned profiles. D) The ratio of nanotunnel extensions (#Nt) to sectioned mitochondria profiles numbers (#Mt) is higher in RyR2<sup>A4860G</sup> vs WT myocytes: 28 ± 9 % (mean and SD, n=588 mitochondria, 51 micrographs,) vs 9 ± 5 % (n= 724 mitochondria, 54 micrographs), 3 hearts each; \*\*\*p<0.0001 (Student's t test). E) The number of mitochondria (# Mt) per area of EM images in longitudinal sections is not different in WT and RyR2<sup>A4860G</sup>: 31 ± 9 (n= 32 areas, 980 mitochondria, 17 cells) vs 28 ± 11 (n= 31 areas, 854 mitochondria, 16 cells); 3 hearts each; p>0.05. F) The average of mitochondria area (μm<sup>2</sup>) in longitudinal section is slightly smaller in the WT than in RyR2<sup>A4860G</sup>: 3.4 ± 0.5 × 10<sup>-2</sup> vs 3.8 ± 1.1 × 10<sup>-2</sup>; \*p<0.05. G) Average of mitochondria area (μm<sup>2</sup>) in cross section is significantly higher in the WT than in RyR2<sup>A4860G</sup>: 3.4 ± 0.5 × 10<sup>-2</sup> (n= 15 areas, 448 mitochondria) vs 2.6 ± 0.5 × 10<sup>-2</sup> (n= 15 areas, 485 mitochondria), 2 hearts; \*\*p<0.001. H) Relative frequency of mitochondria profiles areas in cross sections of WT and RyR2<sup>A4860G</sup> as % of total. In mutant cells there is a clear shift towards small profiles.

the long axis of the tunnel (Fig. 2B, C). This establishes a preferential pathway within the matrix for diffusion along the nanotunnel's long axis. Mitochondrial extensions constituted only of the outer membrane as described in dividing bacteria

341  
342  
343  
344  
345  
346  
347  
348  
349  
350  
351  
352  
353  
354  
355  
356  
357  
358  
359  
360  
361  
362  
363  
364  
365  
366  
367  
368  
369  
370  
371  
372  
373  
374  
375  
376  
377  
378  
379  
380  
381  
382  
383  
384  
385  
386  
387  
388  
389  
390  
391  
392  
393  
394  
395  
396  
397  
398  
399  
400  
401  
402  
403  
404  
405  
406  
407  
408



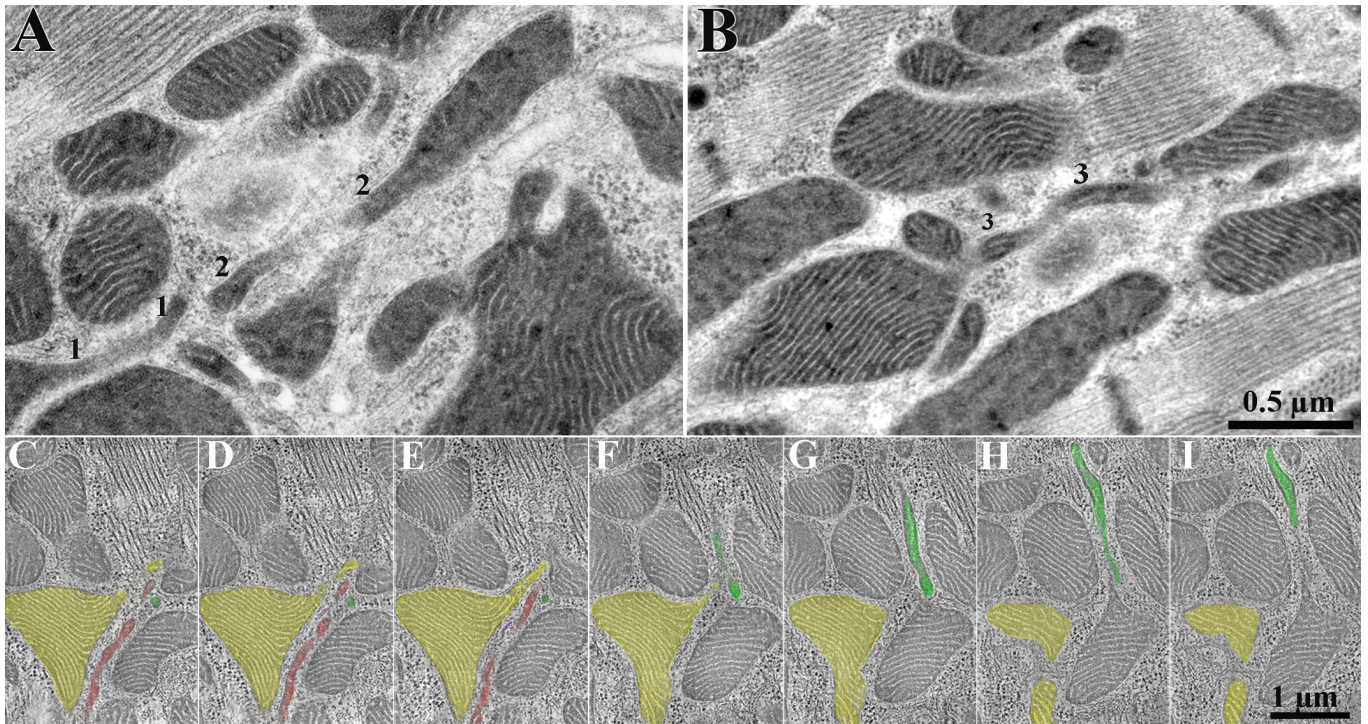


**Fig. 3. The relationship between nanotunnels and small mitochondria profiles imaged in rapidly frozen RyR2<sup>A4860G+/-</sup> myocytes.** A-B) In thin sections, the small profiles 1, 2 and 3 belong to three nanotunnels that are partly included in the section thickness and generate small apparently separated profiles at the edge of the section. C-I) Sequential images taken from a tomogram of a 0.4  $\mu\text{m}$  section (235 images recorded) provide images equivalent to those in thin sections (Movie S1). Three different colors identify profiles that appear continuous in some part of the tomogram but contribute to apparently separate profiles in other views. Microtubules colored in purple (C-G) follow the path of nanotunnel profiles (Movie S1, S7).

are never encountered, indicating that nanotunnels are not simply stretched-out bridging connections between dividing mitochondria that are in the process of moving apart.

The length of nanotunnels profiles varies between 0.7 and 3.6  $\mu\text{m}$  in thin sections. This is likely an underestimate of the real length since the nanotunnels frequently escape from the plane of the thin sections. For the same reason, connections between two mitochondria via nanotunnels are seldom observed, but one is caught in Figure 2C. The frequency of nanotunnel extensions relative to the number of mitochondria is  $\sim 3$  fold higher in mutant compared to the WT, 28 vs 9 (Fig. 2D).

#### The case for a nanotunnels-to-small profiles connection

An immediate question to be considered is whether there is a direct relationship between small mitochondria profiles seen in thin sections and the presence of nanotunnels.

The overall number of mitochondria per area of thin longitudinal section is not different in RyR2<sup>A4860G+/-</sup> and WT (Fig. 2E). The average areas of sectioned mitochondria profiles measured in longitudinal sections is also not very different, 0.36 vs 0.31  $\mu\text{m}^2$  (Fig. 2F). On the contrary, cross sections give data apparently conflicting with those above. First, the average areas of profiles measured in cross sections is smaller by two orders of magnitude than those in longitudinal sections (Fig. 2G). The reason for this apparent discrepancy is that the orientation of both mitochondria and nanotunnels are strongly anisotropic: both are oriented in a longitudinal direction, parallel to the myofibrils' long axis and the length of the mitochondrion contributes significantly to the measured area (Fig. 1A, B). Secondly, the mitochondrial areas in cross sections are significantly smaller in RyR2<sup>A4860G+/-</sup> vs WT (0.025 vs 0.034  $\mu\text{m}^2$ ) (Fig. 2G). The reason for this result is that profiles of mitochondria bodies and of their nanotunnels extensions appear as separate entities in cross sections and each nanotunnel can give rise to small mitochondria profiles at several

points along its length (Fig. 2C). Indeed, the histogram in Fig. 2H, from cross sectional data, shows a large spike in the frequency of mitochondrial profiles with areas of 0.016-0.024  $\mu\text{m}^2$  consistent with that expected from sections cutting at right angles to nanotunnels with the diameter mentioned above (see Fig. 2C) and their presence contributes to the apparent decrease in average mitochondria dimensions in mutants (see Fig. 2G).

#### The complex distribution of nanotunnels and its relationship to microtubules is evidenced by EM tomography and 3D imaging

To directly assess the contribution of nanotunnels to small mitochondria profiles observed in thin section (Fig. 3A, B), we followed the path of nanotunnels through 0.4  $\mu\text{m}$  thick sections using electron tomography (Fig. 3 C-I, Movie S1). In the serial images, three long nanotunnels contribute to several small round mitochondria profiles visible as individual images. Interestingly, microtubules (Figs. 3C-G and 6; Movie S1, S7) follow the path of nanotunnels (see also below).

Mitochondria extending nanotunnels and microtubules were segmented and reconstructed in 3D (Fig. 4; Movies S2 - 4). This more clearly shows that the majority of small mitochondria profiles are sections through nanotunnel extensions. Nanotunnels are quite convoluted and have varied orientations relative to each other and the myofibrils, but they do not show any evidence for direct connections to each other even when they are separated by small distances. Under low magnification, a large zone of intense mitochondria network was reconstructed (Fig. 5, Movie S5). In the volume of the section, nanotunnels pass over each other and other mitochondria forming part of an extensive complex assembly (Fig. 5, Movie S6). Due to limitations of the reconstruction, which does not cover a sufficient depth, it was not feasible to demonstrate direct mitochondrion-to-mitochondrion continuity via nanotunnels.

Ultrathin sections of rapidly frozen cardiomyocytes, as well as electron tomography and 3D reconstructions, showed an abun-



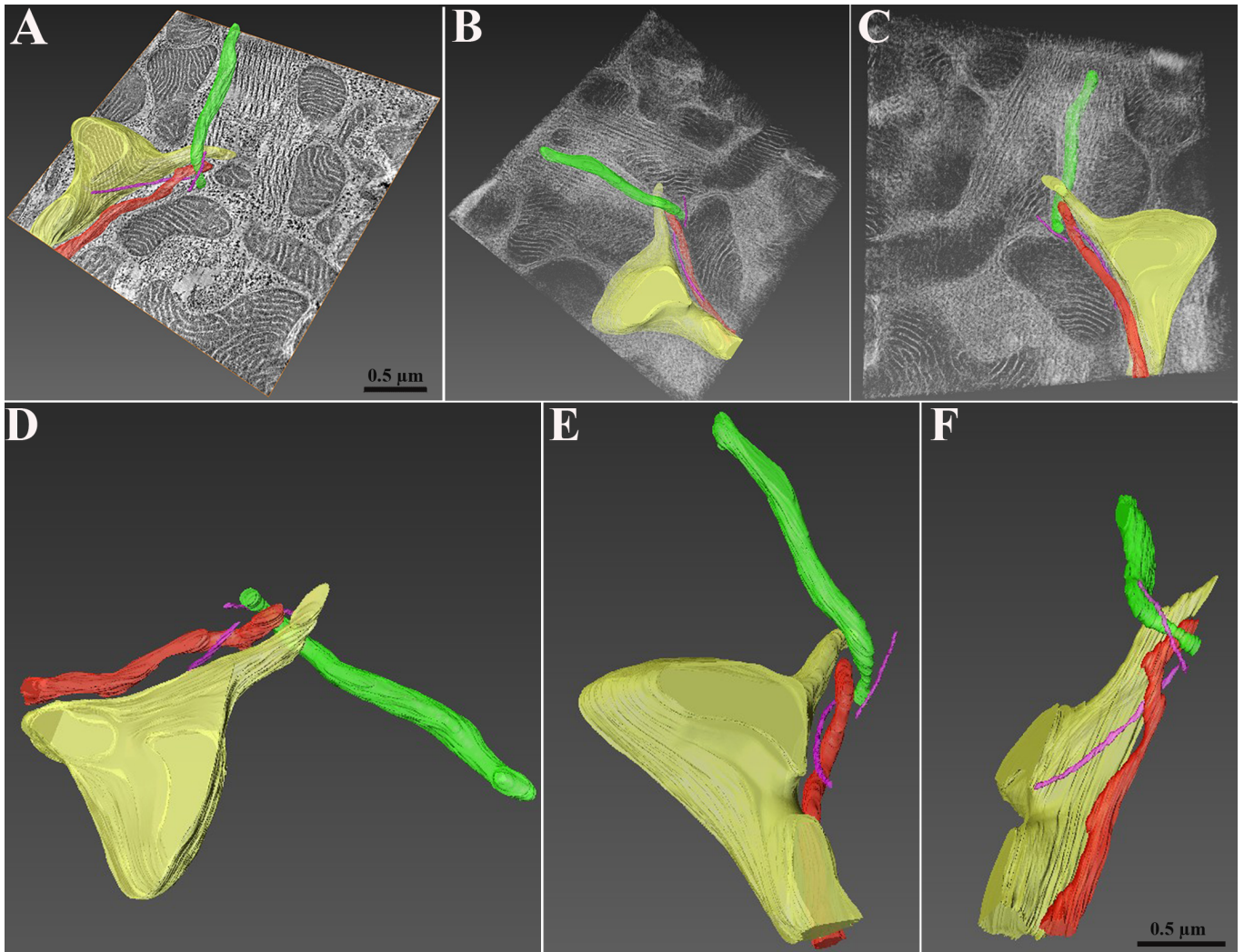


**Fig. 4. 3D Reconstruction of mitochondria nanotunnels in  $RyR2^{A4860G+/-}$ .** A) Orthoslice view of cardiac muscle with mitochondria nanotunnels and microtubules segmented and reconstructed using electron tomograms. Each color identifies a specific mitochondrion (Movie S2), while microtubules are highlighted in purple. B-C) Mitochondria and microtubules are shown in the volume of the section (566 millions voxels) in different orientations. Nanotunnels extend in three dimensions through the volume of the myocyte, passing over each other and appearing as small round mitochondria on the surface of the section (Movie S3). Microtubules follow their profiles. D-F) Three representative orientations emphasize the complexity (Movie S4).

dance of microtubules in close, parallel proximity with nanotunnels (Fig. 6, Movie S7) suggesting that microtubules may contribute to tunneling dynamics. Interestingly, electron micrographs show that cristae in nanotunnels are aligned parallel to the longitudinal axis of the extensions, suggesting the possibility that these structures arise from a pulling action along the microtubules (see Fig. 2C), consistent with the hypothesis that microtubules are involved in this process.

#### Two modes of inter-mitochondria communication with different kinetics

In order to evaluate whether the presence of nanotunnels affects the flow of matrix-targeted soluble fluorescent proteins between mitochondria, we compared exchanges of mtDsRed and mtPA-GFP between mitochondria of isolated WT and  $RyR2^{A4860G+/-}$  cardiomyocytes. mtPA-GFP was photoactivated within 2-5 small square areas ( $25 \mu m^2$ ) per cell resulting in simultaneous bleaching of mtDsRed in the same area (Fig. 7A). During the time of recording (165 cycles at 3s intervals), the mtPA-GFP fluorescence decays in the photoactivated (PA) areas while small positive spots appear within a few microns (Fig. 7A). Since the proteins are within the mitochondria matrix this must indicate

flow through some mitochondrial extensions and/or exchanges between mitochondria.

The overall fluorescence decay in the PA areas is a direct measure of the rate of loss of mtPA-GFP and gives an indication of the movement of matrix proteins from one set of mitochondria to others. The mtPA-GFP decay is significantly slower in heterozygotes than in WT cells. At 445s after a 15 s activating pulse (Fig. 7B and C) the fluorescence has decayed by 12 % of the value at photoactivation in heterozygotes compared to 29 % in WT.

Analysis of individual acceptor organelles outside the PA areas simultaneously detected the time course of two indicators for matrix exchange between organelles: the gain of mtPA-GFP from a donor and the loss of unbleached mtDsRed to the same donor. The time course of the mixing kinetics shows the green fluorescence increasing while the red one declines in the acceptor within the same time interval, until equilibrium is reached (Fig. 8). To compare dynamic rates and geometric factors, we arbitrarily divided the matrix mixing events into two groups: "slow" events that require  $>30$  s (30 to 111 s in WT and 30 to 183 s in mutant) to reach equilibrium and "fast" events, requiring  $<30$  s (Fig. 8). The percentage of slow events is significantly higher in the mutant

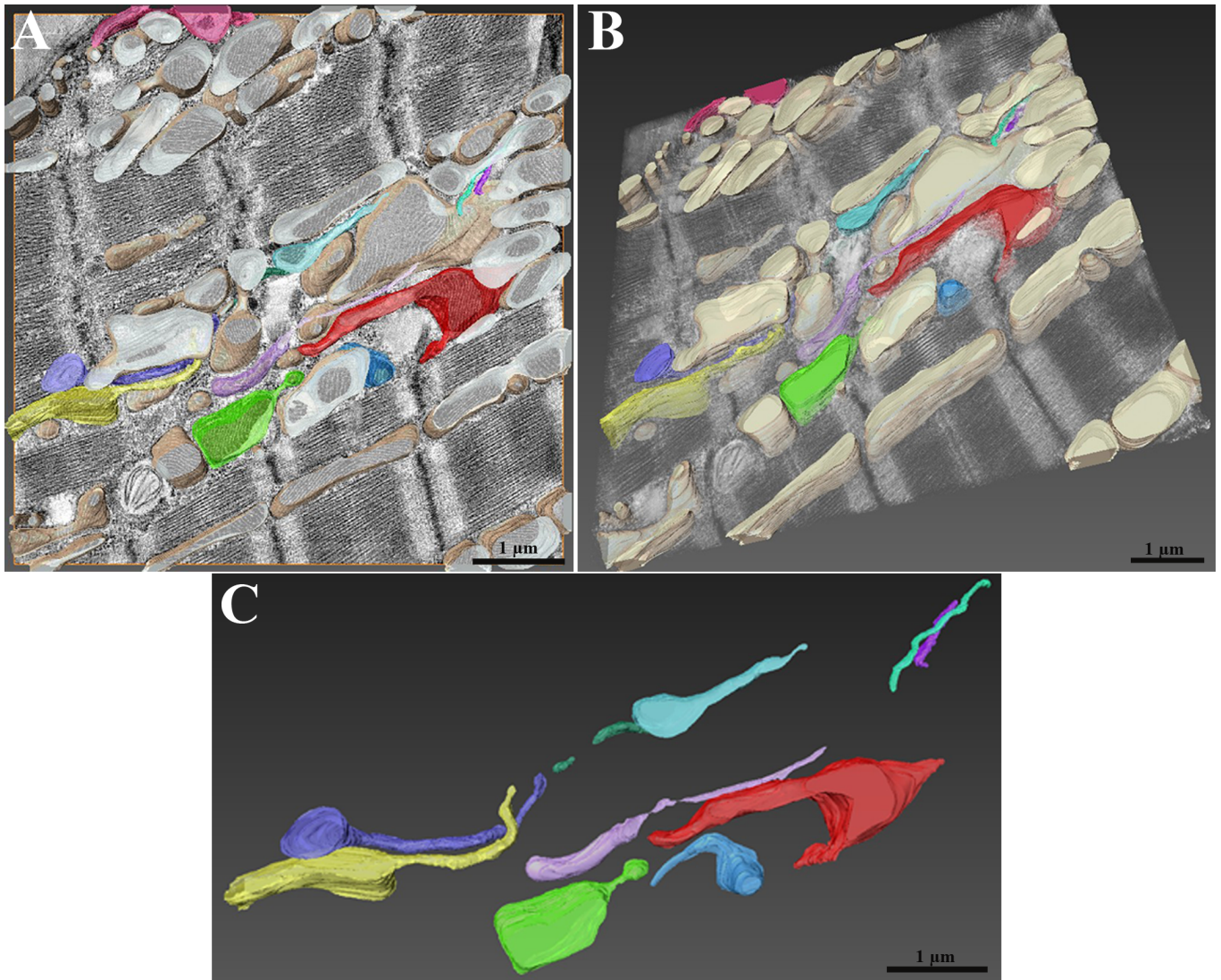


**Fig. 5. Complexity of nanotunnels dispositions in a large sectional area of RyR2<sup>A4860G</sup>±.** A tomogram was recorded at lower STEM magnification (14000x) to reconstruct a large area of intense mitochondria nanotunneling activity. Mitochondria not extending nanotunnels are colored in pale brown, mitochondria extending nanotunnels are highlighted by different colors. A) Orthoslice view of the myocyte with mitochondria 3D reconstruction (Movie S5). B) View of mitochondria in the myocyte volume (255 million voxels) showing the complex arrangement in a crowded area (Movie S6). C) 3-D model of nanotunnels showing their variability on length: some extend over several microns.

than in WT (56% vs 24%) (Fig. 8D), in good agreement with the slower overall fluorescence decay in the RyR2<sup>A4860G</sup>± (Fig. 7C).

Events also differ in terms of the distance between the edges of the PA areas and the site of appearance of new mtPA-GFP spots presumably representing acceptor mitochondria. Considering that in the electron micrographs the length of mitochondria nanotunnel averaged between 0.6 - 3.6 μm, we decided that a threshold of ≥ 1 μm is a sufficient distance to indicate a communication requiring the presence of a nanotunnel in events at "long distance" (Fig. 8 A, B, Movie S8). "Short distance" events, by contrast, indicate increases in mtPA-GFP intensity at <1 μm distance from the PA area or a photoactivated neighboring mitochondrion (Fig. 8 C, Movie S9). We estimated the frequency of "long distance" events in a subset of cells. Long distance events are significantly more frequent in RyR2<sup>A4860G</sup>± cells than in WT: 43% vs 21% (Fig. 8 D) with a distance range of 1 to 6 μm. This is in general agreement with the higher frequency of nanotunnels in RyR2<sup>A4860G</sup>± cells.

If communication via nanotunnels affects the rate of fluorescent protein exchange, we should find some relationship between the rate of matrix mixing and the relative positions of donor and acceptor mitochondria. Close to 100% of long distance events in mutant (27 out of 28) and WT (13 out of 14) show slow mixing kinetics. Short distance events have predominantly, although not exclusively, fast kinetics (73 and 76% of total respectively in mutant and WT). Figure 8 compares examples of two long distance events, where the transfer of mtPA-GFP is relatively slow (≥40 s to reach the equilibrium in this case), with two short distance events, where the mixing kinetics are either fast (20 s) or slow (60 s). These are in agreement with the general slow exchange in long distance events and the mixed slow/fast exchange in short distance event. In conclusion, the kinetics of long distance and short distance events are essentially similar in WT and mutant, but their frequencies are different suggesting that the overall slower transmission in the latter is due to the increased frequency of long distance, slower events.

Direct observations of mtPA-GFP movement along nanotunnels were infrequent. A combination of the small size of the

681  
682  
683  
684  
685  
686  
687  
688  
689  
690  
691  
692  
693  
694  
695  
696  
697  
698  
699  
700  
701  
702  
703  
704  
705  
706  
707  
708  
709  
710  
711  
712  
713  
714  
715  
716  
717  
718  
719  
720  
721  
722  
723  
724  
725  
726  
727  
728  
729  
730  
731  
732  
733  
734  
735  
736  
737  
738  
739  
740  
741  
742  
743  
744  
745  
746  
747  
748

749  
750  
751  
752  
753  
754  
755  
756  
757  
758  
759  
760  
761  
762  
763  
764  
765  
766  
767  
768  
769  
770  
771  
772  
773  
774  
775  
776  
777  
778  
779  
780  
781  
782  
783  
784  
785  
786  
787  
788  
789  
790  
791  
792  
793  
794  
795  
796  
797  
798  
799  
800  
801  
802  
803  
804  
805  
806  
807  
808  
809  
810  
811  
812  
813  
814  
815  
816



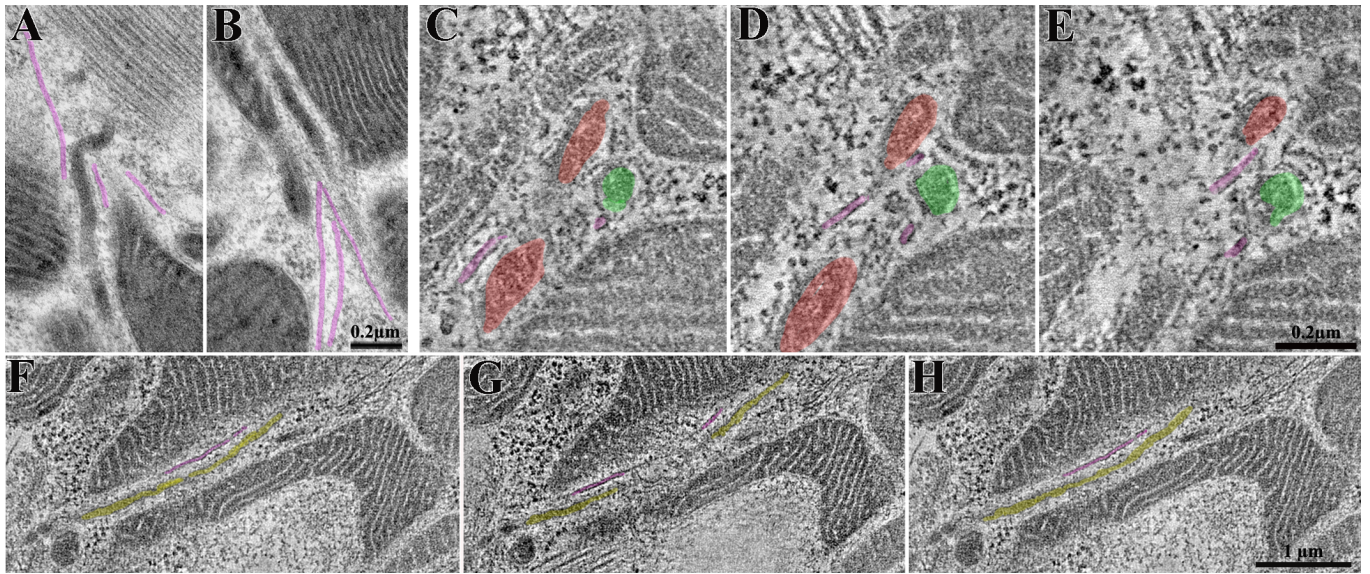


**Fig. 6. Microtubules apparently guide nanotunnels.** A-B) Ultrathin section of rapidly frozen cardiomyocyte. Microtubules (in purple) are very close to mitochondria profiles and are oriented following the direction/orientation of nanotunnels. C-H) Selected images from two tomograms showing microtubules that accompany nanotunnels (red, green in C-E and yellow in F-H) (Movie S7).

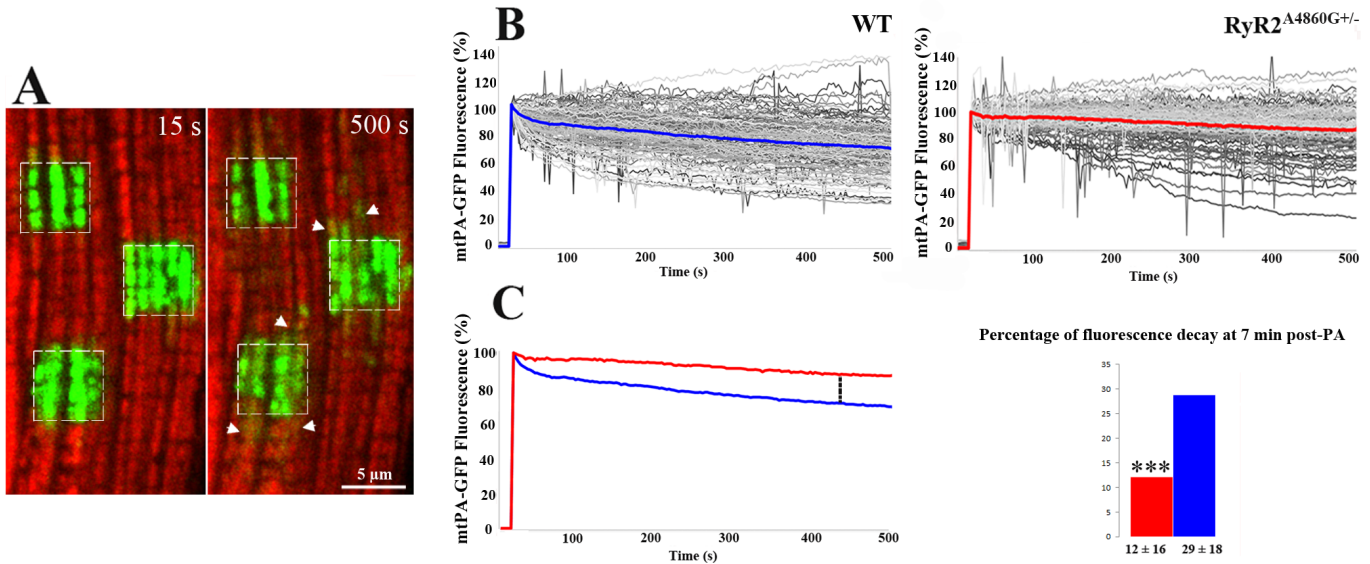


**Fig. 7. mtPA-GFP fluorescence decay in WT and RyR2<sup>A4860G+/-</sup> cardiomyocytes.** A) Representative WT cardiomyocyte showing PA areas (squares) at 15 s from irradiation and at the end of recording (500 s). The mtPA-GFP fluorescence decays in the selected areas while small positive spots (arrowheads) appear in their vicinity. B) Intensity of mtPA-GFP fluorescence signal in PA areas normalized to PA peak value during 500s of recording. Gray curves represent individual regions, blue and red the average in WT and heterozygotes respectively. C) Left: Direct comparison of the two average traces. The decay is faster in WT. Right: At 445s post-PA, percentage decay of signal is significantly smaller in heterozygote (red) than in WT (blue):  $12 \pm 16$  (mean, SD) vs  $29 \pm 18$ ,  $p^{***} < 0.0001$ . 36 cells, 109 PA areas, from 3 RyR2<sup>A4860G+/-</sup> mice and 53 cells, 126 PA areas from 4 WT mice.

nanotunnel and the rapidity of matrix protein movement along it are the probable causes. Figures 8B and 9 offer rare direct views of nanotunnel activity, with the movement of small mtPA-GFP boluses along a single narrow path  $\sim 5 \mu\text{m}$  long (Fig. 9 C, Movie S10).

To investigate the cause of the slow rate of matrix mixing between mitochondria located at longer distances from each other, the rate of matrix flow along nanotunnels needs to be considered. The ratio between the time of the first appearance of green fluorescence in a distant mitochondrion and its distance from the PA area is quite variable indicating a possible rate of flow between 4 and 121 nm/sec (mean  $43 \pm 34$  nm/sec). Thus, the influence on mitochondria mixing rates by the rate of

diffusion along the nanotunnels is quite variable and may not be the limiting factor.

A final observation is that during imaging of  $>200$  PA areas for 500s each, no migration of mitochondria was detected. Each mitochondrion has a well visible imprint in the confocal images once its mtPA-GFP is activated. Migration of an entire mitochondrion from the activated area would leave behind a noticeable local dip in fluorescence and would appear as a large positive spot elsewhere. This clearly demonstrates the basic stability of the mitochondria positioning between the myofibrils.

### Discussion

The unexpected effect of the RyR2A4860G mutation on mitochondria morphology and kinetics, provide a novel approach for

953  
954  
955  
956  
957  
958  
959  
960  
961  
962  
963  
964  
965  
966  
967  
968  
969  
970  
971  
972  
973  
974  
975  
976  
977  
978  
979  
980  
981  
982  
983  
984  
985  
986  
987  
988  
989  
990  
991  
992  
993  
994  
995  
996  
997  
998  
999  
1000  
1001  
1002  
1003  
1004  
1005  
1006  
1007  
1008  
1009  
1010  
1011  
1012  
1013  
1014  
1015  
1016  
1017  
1018  
1019  
1020

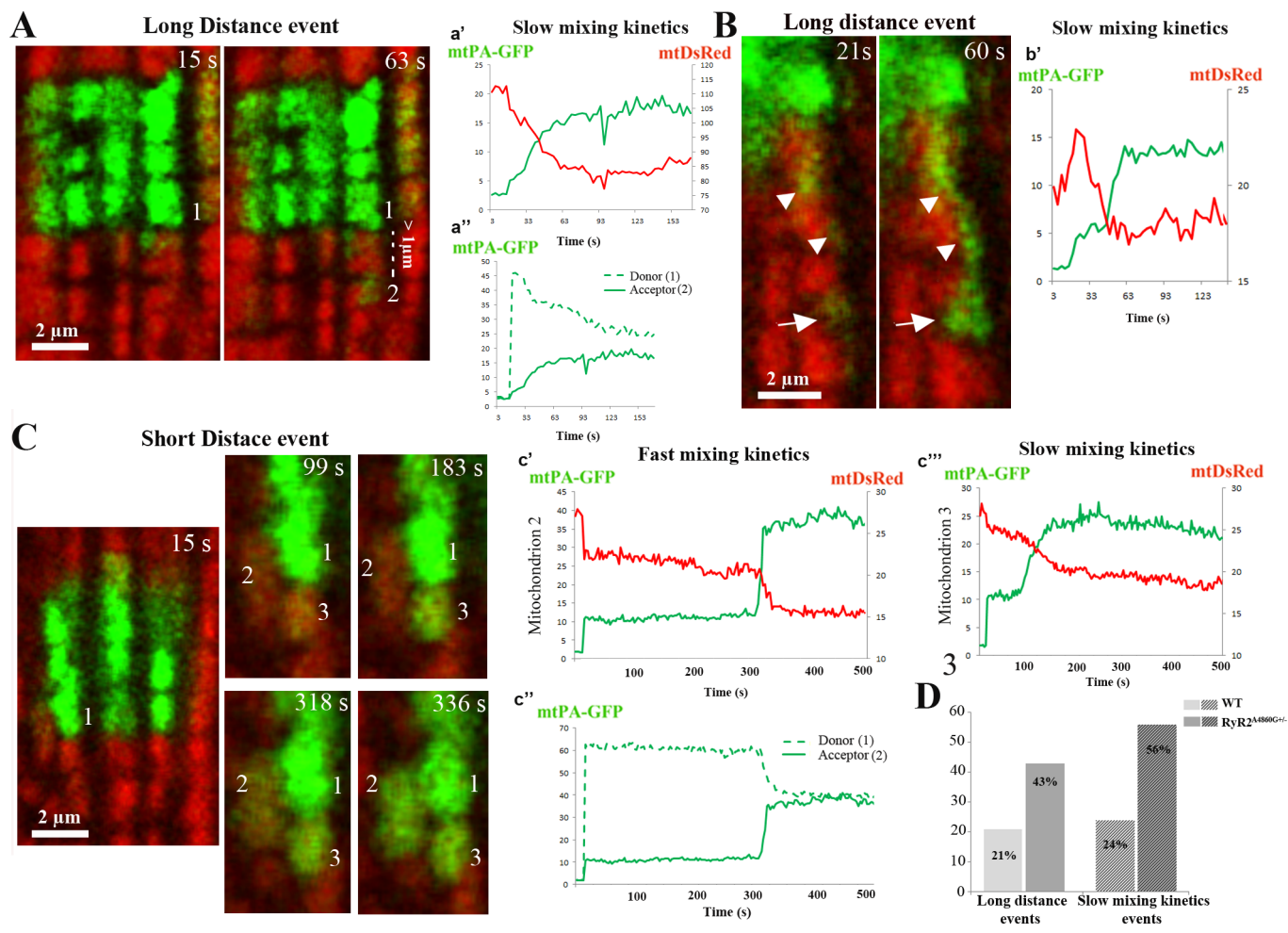


**Fig. 8. Long and short distance events and mixing kinetics.** Representative images and examples of mixing kinetics events in WT selected for their visibility. A) Long distance event where an increase in mtPA-GFP intensity is detected at  $\geq 1 \mu\text{m}$  from the PA area. #1 Mitochondrion, located in the PA area, slowly donates mtPA-GFP fluorescence to #2 mitochondrion. a') Increase in mtPA-GFP fluorescence and decrease in mtDsRed of #2 mitochondrion occur with the same time course. Equilibrium is reached after 45s. a'') The presumed donor, #1 mitochondrion, loses mtPA-GFP fluorescence in parallel to an increase in the acceptor (#2). B) Rare view of a GFP labeled nanotunnel (arrowheads) that reaches a mitochondrion over a long ( $\sim 6 \mu\text{m}$ ) distance (arrow, Movie S8). b') Fairly slow exchange of mtPA-GFP and mtDsRed (40s to equilibrium). C) Two short distance events displaying different mixing kinetics: fast, between mitochondria #1 and #2 and slow, between a not well identified mitochondrion in the PA area and #3 (Movie S9). c') The fast mixing kinetics in #2 mitochondrion leads to equilibrium in 18s, mtPA-GFP and mtDsRed fluorescence are mirror images of each other. c'') mtPA-GFP fluorescence in the presumptive donor and acceptor (mitochondria 1 and 2). c''') Slow mixing kinetics in #3 mitochondrion, that leads to equilibrium in 84s. D) The percentage of both long distance and slow mixing kinetics events are increased in RyR2<sup>A4860G+/-</sup> vs in WT. Data from 82 events, 13 cell, 34 PA areas, 3 mice for WT and 66 events, 14 cells, 38 PA areas, 4 mice for RyR2<sup>A4860G+/-</sup>.

the differentiation of two modalities of intermitochondria matrix exchanges: 1) at direct large contact sites; 2) via narrow nanotunnels between distant organelles (12), both occurring without movement of the individual organelles. The static EM images indicate an apparent and intense activation of nanotunneling activity in the mutant which is surprisingly linked to depression rather than enhancement of intermitochondria matrix exchange rates: in mutant cells the overall frequency of exchange events is slightly reduced and the relative incidence of long distance, intrinsically slower events is higher. The combination of the two factors may be at the basis of the slower overall rate of matrix exchange. However it cannot be excluded that the mutation causes a primary functional defect in the mixing. This work establishes a well-defined level of mitochondrial behavior in normal myocardium that can be utilized as a platform for comparison altered behavior in this mutation as well as in other cardiac pathologies.

In both WT and mutant cells, exchange events occur at a relatively low frequency in comparison to the frequency of sites at which mitochondria are closely apposed to each other at

kissing junctions and/or presumably at the end of nanotunnel extensions. Therefore the initiation of an event must involve some stochastic transition in the relationship between the two interacting mitochondria. One possibility (11) is that an exchange is initiated by an actual fusion event which permits direct mixing of matrices. A second possibility (12) is that the membranes at kissing junctions become permissive to direct movements of proteins from one organelle to the other. Both hypotheses have some intrinsic weaknesses. In the case of fusion the problem is that the matrix exchange is relatively slow, even considering the possible negative effect of matrix space complexity. In the case of kissing junctions, a yet unexplored mechanism by which opening of pores in both outer and inner membranes are coordinated must be provided.

Regardless of the mechanism by which communication is established (either fusion or gating of kissing junctions) the difference in the rate of exchange between long distance events involving nanotunnels and those at close range involving contacts between the main body of mitochondria is most likely to be

1021  
1022  
1023  
1024  
1025  
1026  
1027  
1028  
1029  
1030  
1031  
1032  
1033  
1034  
1035  
1036  
1037  
1038  
1039  
1040  
1041  
1042  
1043  
1044  
1045  
1046  
1047  
1048  
1049  
1050  
1051  
1052  
1053  
1054  
1055  
1056  
1057  
1058  
1059  
1060  
1061  
1062  
1063  
1064  
1065  
1066  
1067  
1068  
1069  
1070  
1071  
1072  
1073  
1074  
1075  
1076  
1077  
1078  
1079  
1080  
1081  
1082  
1083  
1084  
1085  
1086  
1087  
1088



1089  
1090  
1091  
1092  
1093  
1094  
1095  
1096  
1097  
1098  
1099  
1100  
1101  
1102  
1103  
1104  
1105  
1106  
1107  
1108  
1109  
1110  
1111  
1112  
1113  
1114  
1115  
1116  
1117  
1118  
1119  
1120  
1121  
1122  
1123  
1124  
1125  
1126  
1127  
1128  
1129  
1130  
1131  
1132  
1133  
1134  
1135  
1136  
1137  
1138  
1139  
1140  
1141  
1142  
1143  
1144  
1145  
1146  
1147  
1148  
1149  
1150  
1151  
1152  
1153  
1154  
1155  
1156

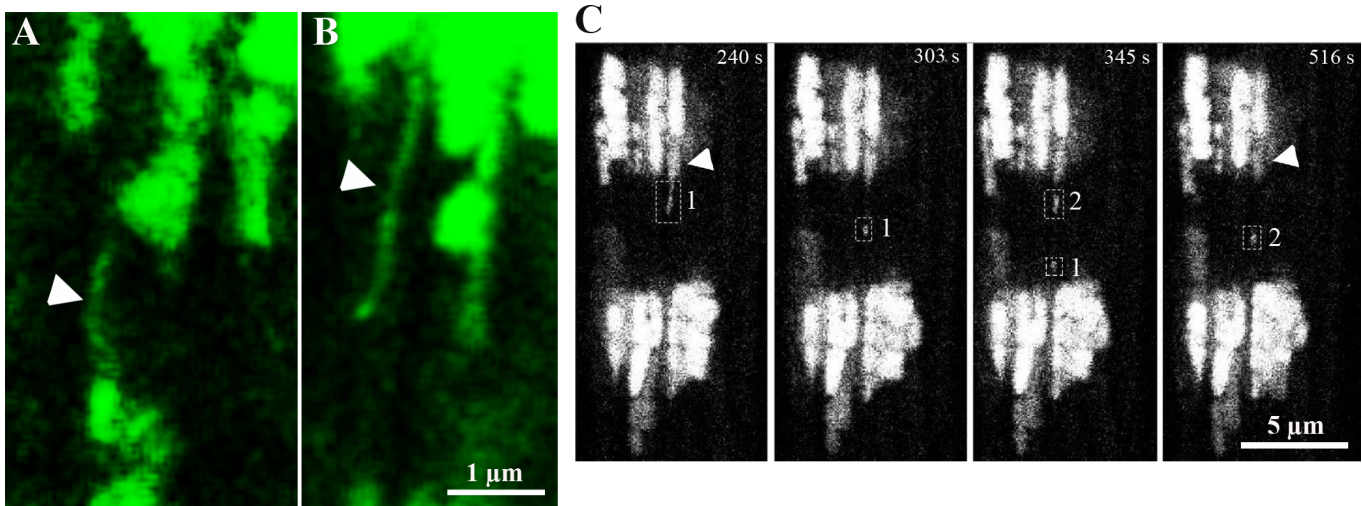


**Fig. 9. Nanotunnel activities in live cardiomyocytes.** A-B) Representative images of nanotunnels highlighted by their content of mtPA-GFP (arrowheads) in RyR2<sup>A4860G/+</sup> (A) and WT (B) cardiomyocytes. C) Sequential movement of green fluorescence along a nanotunnel extension in a RyR2<sup>A4860G/+</sup> cardiomyocyte with parallel loss from a donor (arrowhead) during 276s recording. Initially (left image), a narrow line of fluorescence (rectangle 1) is close to the PA area. After 99 s the signal has moved away progressing further to a total distance of ~ 5 μm reaching the 2<sup>nd</sup> PA area (at 345 s) moving at 48 nm/sec, while a new fluorescence (2) is released from the donor and it also moves away from the PA area (at 516 s) (Movie S10).

related to differences in their geometry. In 3D reconstructions, nanotunnels, even where crowded in a small space, do not seem to make frequent contacts with each other and with large mitochondria. This may indicate that the sites of communication are near the nanotunnel tips. The orientation of cristae and matrix spaces seem to facilitate flow along the length of the nanotunnels, but given the small diameter, the area of contact at the tips is quite limited thus providing a restriction for matrix flow. Cell to cell communication via long narrow extensions are not unique to cardiac mitochondria. Free bacteria, also communicate via short connecting tunnels (25) and so do higher cells (26), although in the latter case the communication may be restricted to the ferrying of organelles.

One interesting question is whether exchanges via nanotunnels depend on the availability of preformed elongated paths or whether nanotunnels develop in the process of an exchange event. The high frequency of nanotunnels in mutant myocytes may favor the former hypothesis, but unfortunately live images cannot solve the question because a nanotunnel is visible only when filled with activated mtPA-GFP. Regardless of the moment of formation, it is likely that nanotunnels are generated by an active pull of the mitochondria along microtubules. The frequent nanotunnels-microtubules appositions and the orientation of cristae is just what one would expect from such a mechanism. Incidentally, this possible mechanism of nanotunnel generation implies a mechanical anchorage of mitochondria (via tethers) that lets them resist the pull, consistent with lack of evidence for mitochondria migrations in live images.

Short and long distance matrix exchanges between cardiac mitochondria allow the necessary communication without need of disrupting the original position of the organelles. In skeletal muscle of some species the dichotomy between a large mitochondrion body and long thin extensions is not as marked as in cardiac muscle, because the whole mitochondrion is thin and elongated (27). It is not known how actively these mitochondria expand/retract along the narrow spaces available, but clearly they maintain a specific relationship to the triads.

The frequencies of small mitochondria profiles and nanotunnels are higher by a factor of ~ 1.5 and ~3 respectively in mutant vs WT myocytes. The EM data illustrate that each nanotunnel and/or shorter mitochondria extension, contribute to several apparently separate small profiles in thin sections. If

each of the additional nanotunnels in mutant myocytes happened to be transected by the section at 1-2 sites, that in itself would explain the increased frequency of small profiles following the RyR2 mutation. Thus although some fission activity may occur in mutant cells, this is probably not a common event. By contrast, in a separate RyR2 mutation that results in gain of RyR2 release function and eventually in heart failure (28), we observed very extensive fragmentation of mitochondria and no nanotunneling. Therefore, nanotunneling is not a necessary prelude to fragmentation. In non muscle cells fusion/fission events are coupled to large mitochondrial migrations (2). The indication from this work is that cardiac mitochondria do not need to migrate in order to communicate with each other and mitochondria apparently maintain their original position, despite the large Ca<sup>2+</sup> imbalances. This is somewhat surprising in view of the fact that in non muscle cells large mitochondrial movements and/or fission occur under other related conditions. However, even within striated muscles, mitochondria are not necessarily permanently immobilized. Dispositions of mitochondria is highly variable when one considers examples from a variety of vertebrates (29); their positioning is developmentally regulated (5); and they may acquire freedom of movement under certain pathological conditions (28, 30, 31).

The relationship between the altered Ca<sup>2+</sup> homeostasis due to the RyR2<sup>A4860G/+</sup> mutation and the induction of nanotunneling is not clear, unless it is mediated by an increase activity of transport along microtubules, that may be affected by Ca<sup>2+</sup>.

**Materials and Methods**

**Experimental Animals**

The RyR2<sup>A4860G/+</sup> mouse was generated and maintained as previously described (1).

**2D Electron microscopy**

Heterozygous and WT hearts of 7 months old mice were perfused and fixed with 6 % glutaraldehyde in 0.1 M sodium cacodylate buffer (pH 7.4), kept at 4 °C and small bundles of ventricular wall muscles processed for standard thin section electron microscopy (28). Fiji program (NIH) was used for morphometric analysis of randomly collected images. Cross sections (mag. 19,300x) and longitudinal sections (mag. 26,300x) were used to measure areas of mitochondria profiles and count frequency of nanotunnels.

**Electron tomography and 3D reconstruction**

Previously fixed (see above) small cardiac bundles were rapidly frozen using a high-pressure freezing system (HPM 010), free substituted in 100% acetone, 0.1% uranyl acetate and embedded at -50° C in lowicryl (HM-20). Resin was polymerized with 348 nm light for 48 h at low temperatures and 48 h at 25° C. The surfaces of thick sections (0.4 μm) were labeled with

1157  
1158  
1159  
1160  
1161  
1162  
1163  
1164  
1165  
1166  
1167  
1168  
1169  
1170  
1171  
1172  
1173  
1174  
1175  
1176  
1177  
1178  
1179  
1180  
1181  
1182  
1183  
1184  
1185  
1186  
1187  
1188  
1189  
1190  
1191  
1192  
1193  
1194  
1195  
1196  
1197  
1198  
1199  
1200  
1201  
1202  
1203  
1204  
1205  
1206  
1207  
1208  
1209  
1210  
1211  
1212  
1213  
1214  
1215  
1216  
1217  
1218  
1219  
1220  
1221  
1222  
1223  
1224

1225 ~ 15 nm gold particles. Tilt series were collected at 200 keV accelerating  
1226 voltage using FEI Tecnai F20 transmission electron microscope reaching max  
1227 negative and positive tilts of 68°. Images in STEM mode were captured using  
1228 a Fischione HAAD camera. 264 and 112 images were used for high (28000)  
1229 and low (14000) magnification tomograms using IMOD (version 4.7). Videos  
1230 were created using series of snapshots made in IMOD and importing those  
1231 images into movie-making software, Videomach (from www.gromada.com).  
1232 Surface segmentation of the organelles was obtained by outlining the profile  
1233 in AMIRA 5.6 3D software (FEI). The volumes were reconstructed using direct  
1234 volume rendering of 3D images with shadings (Volren).

#### Adenovirus infection, cardiomyocytes isolation

1234 Hearts of seven-eight months old mice were infected with adenovirus  
1235 carrying mtDsRed and mtPA-GFP cDNA by 4-5 intramyocardial injections of  
1236  $5 \times 10^8$  PFU of Adenovirus in total volumes of 20  $\mu$ l. After 7 days, hearts were  
1237 subjected to enzymatic perfusion to isolate adult cardiomyocytes. Cells were  
1238 plated and incubated for 1-2h in plating medium (MEM, 10% calf serum,  
1239 penicillin 100U/ml, ATP 2mM, glutamine 2mM, BDM 10mM) followed by  
1240 culture medium (MEM, 0.1% BSA, penicillin 100U/ml, glutamine 2mM, BDM  
1241 10mM, 1% ITS (5 $\mu$ g/ml insulin, 5 $\mu$ g/ml transferrin, 5ng/ml selenium) all at  
1242 37°C and 2% CO<sub>2</sub>.

#### Live confocal microscopy

1242 Live imaging approach follows seminal experimental guidelines developed  
1243 and implemented by Dr. Veronica Eisner (Dept de Biología Celular y  
1244 Molecular, Facultad de Ciencias Biológicas, Pontificia Universidad Católica de  
1245 Chile) which is the subject of a separate publication. Imaging of isolated  
1246 cells was performed, within 12 h after cardiomyocytes isolation, in 0.25%  
1247 BSA with the addition 10mM BDM (2,3 Butanedione monoxime) to inhibit

- 1248 1. Benard G, Bellance N, James D, Parrone P, Fernandez H, Letellier T, Rossignol R (2007) Mitochondrial bioenergetics and structural network organization. *J Cell Sci* 120(Pt 5): 838-848.
- 1249 2. Liu X, Weaver D, Shirihai O, Hajnóczky G (2009) Mitochondrial 'kiss-and-run': interplay between mitochondrial motility and fusion-fission dynamics *EMBO J* 28(20): 3074-3089.
- 1250 3. Wang C, Du W, Su QP, Zhu M, Feng P, Li Y, Zhou Y, Mi N, Zhu Y, Jiang D1,2, Zhang S2, Zhang Z1,2, Sun Y3,4, Yu L1,2, et al. (2015) Dynamic tubulation of mitochondria drives mitochondrial network formation. *Nature Cell Res* 25:1108-1120.
- 1251 4. Glancy B, Hartnel L M, Malide D, Yu Z-X, Combs C A, Connelly PS, Subramaniam S, Balaban RS (2015) Mitochondrial reticulum for cellular energy distribution in muscle. *Nature* 523, 617-620 doi:10.1038/nature14614.
- 1252 5. Boncompagni S, Rossi A E, Micaroni M, Beznoussenko G, Polishchuk RS, Dirksen RT, Protasi F (2009) Mitochondria are linked to calcium stores in striated muscle by developmentally regulated tethering structures. *Mol Biol Cell* 20(3):1058-67.
- 1253 6. Ainbinder A, Boncompagni S, Protasi F, Dirksen RT (2015) Role of Mitofusin-2 in mitochondrial localization and calcium uptake in skeletal muscle. *Cell Calcium*. 57(1):14-24.
- 1254 7. Rossi AE, Boncompagni S, Wei L, Protasi F, Dirksen RT (2011) Differential impact of mitochondrial positioning on mitochondrial Ca<sup>2+</sup> uptake and Ca<sup>2+</sup> spark suppression in skeletal muscle. *Am J Physiol Cell Physiol* 301(5):C1128-39.
- 1255 8. Konstantinidis K, Lederer W J, Rizzuto R, Kitsis RN (2012) Mitofusin 2 Joins the Sarcoplasmic Reticulum and Mitochondria at the Hip to Sustain Cardiac Energetics. *Circ Res* 111(7): 821-823.
- 1256 9. Friedman, J.R, Nunnari J (2014). Mitochondrial form and function. *Nature* 505, 335-343.
- 1257 10. Shirihai, OS, Song, M, & Dorn GW II (2015) How Mitochondrial Dynamism Orchestrates Mitophagy. *Circ Res* 116, 1835-1849 (2015).
- 1258 11. Eisner V, Linares G, Hajnóczky G (2014) Mitochondrial fusion is frequent in skeletal muscle and supports excitation-contraction coupling. *J Cell Biol* 205:2 179-195.
- 1259 12. Huang X, Sun L, Ji S, Zhao T, Zhang W, Xu J, Zhang J, Wang Y, Wang X, Franzini-Armstrong C, Zheng M, Cheng H (2013) Kissing and nanotunneling mediate intermitochondrial communication in the heart. *Proc Natl Acad Sci* 110: 2846-2851.
- 1260 13. Picard M, McManus M J, Csordás G, Várnai P, Dorn II G W, Williams D, Hajnóczky G, Wallace D C (2015) Trans-mitochondrial coordination of cristae at regulated membrane junctions. *Nature comm* 6: 6259-61.
- 1261 14. Dedkova, E N, Blatter, L A (2013) Calcium signaling in cardiac mitochondria. *J Mol Cell Cardiol* 58:125-133 doi:10.1016/j.yjmcc.2012.12.021.
- 1262 15. Frank S, Gaume B, Bergmann-Leitner E S, Leitner W W, Rober E G, Catez F, Smith C L, Youle R J (2001) The Role of Dynam-Related Protein 1, a Mediator of Mitochondrial Fission, in Apoptosis. *Dev Cell* 1(4): 515-525.
- 1263 16. Cereghetti G M, Stangherlin A, Martins de Brito O, Chang C R, Blackstone C, Bernardi P, Scorrano L (2008) Dephosphorylation by calcineurin regulates translocation of Drp1 to mitochondria. *Proc Natl Acad Sci* 105:1583-1588.
- 1264 17. Macaskill, A. F., Rinholm, J. E., Twelvetrees, A. E., Arancibia-Carcamo, I. L., Muir, J., Fransson, A., Aspenstrom, P., Attwell, D., and Kittler, J. T. (2009). Miro1 is a calcium sensor

1293 contraction using a laser scanning microscope (LSM 780, Carl Zeiss), exciting  
1294 488nm (mtPA-GFP) and 568nm (mtDsRed) with 63x/1.4 NA Apoplan oil  
1295 objective. To photoactivate mtPA-GFP and photobleach mtDsRed, a pulsed  
1296 laser beam (760 nm, Chameleon; Coherent) was applied within selected 2-5  
1297 square areas (25  $\mu$ m<sup>2</sup>) in two-photon mode. Fluorescence of activated mtPA-  
1298 GFP and of mtDsRed was recorded for ~500 seconds (s) (165 cycles of 3s).

#### Live imaging analysis

1299 We analyzed the time dependence of mtPA-GFP fluorescence decay  
1300 within each square by determining the ratio of mtPA-GFP/mtDsRed fluores-  
1301 cence levels at each successive 3 s time points and normalizing it to the value  
1302 at the time of photoactivation. Spectralyzer software (customer designed)  
1303 was used to analyze the green and red intensity levels for individual sites  
1304 where spread of activated PA-GFP outside the square was detected. The  
1305 resulting graphs were used to define the rate of reciprocal exchange at each  
1306 separate event. The position of each individual event (near or far) from the  
1307 nearest possible site of origin, were determined and compared with the rate  
1308 of exchange.

#### Statistics

1309 All data are expressed as mean  $\pm$  SD. Significance was calculated by  
1310 Student's t test.

1310 **Acknowledgments.** We thank Dr. Veronica Eisner for suggestions and  
1311 practical advice in the live experiment studies, David Weaver for help in  
1312 some experimental set up and Marina Scardigli for substantial help in the  
1313 3D reconstructions. Supported by NIH grant 2PO1 AR 052354-06A1 to P.D.  
1314 Allen (Clara Franzini-Armstrong, Core leader) and RO1 DK051526 to G.H.

- 1315 for glutamate receptor-dependent localization of mitochondria at synapses. *Neuron* 61, 541-555.
- 1316 18. Saotome, M., Sufuilina, D., Szabadkai, G., Das, S., Fransson, A., Aspenstrom, P., Rizzuto, R., and Hajnóczky, G. (2008). Bidirectional Ca<sup>2+</sup>-dependent control of mitochondrial dynamics by the Miro GTPase. *Proc Natl Acad Sci U S A* 105, 20728-20733.
- 1317 19. Wang, X., and Schwarz, T. L. (2009). The mechanism of Ca<sup>2+</sup>-dependent regulation of kinesin-mediated mitochondrial motility. *Cell* 136, 163-174.
- 1318 20. Sharma, V.K., Ramesh, V., Franzini-Armstrong, C, Sheu, S-S (2000) Transport of Ca from the sarcoplasmic reticulum to mitochondria in rat ventricular myocytes. *J. Bioenergetics Biomembrane*. 32:97-104.
- 1319 21. Eisner V, Csordás G, Hajnóczky G (2013) Interactions between sarco-endoplasmic reticulum and mitochondria in cardiac and skeletal muscle - pivotal roles in Ca<sup>2+</sup> and reactive oxygen species signaling. *J Cell Sci*.126 (Pt 14):2965-78.
- 1320 22. Boncompagni S, Rossi AE, Micaroni M, Hamilton SL, Dirksen RT, Franzini-Armstrong C, Protasi F (2009). Characterization and temporal development of cores in a mouse model of malignant hyperthermia. *Proc Natl Acad Sci U S A* 106(51):21996-2001.
- 1321 23. Duhuram W J, Aracena-Parks P, Long C,\* Rossi A E, Goonasekera S A, Boncompagni S, Galvan D L, Gilman C P, Baker M, Shirokova N, Protasi F, Dirksen R, Hamilton S (2008) RyR1 S-Nitrosylation Underlies Environmental Heat Stroke and Sudden Death in Y522S RyR1 Knock-in Mice. *Cell* 133(1):53-65.
- 1322 24. Zhao Y-T, Valdivia C R, Gurrola G B, Poversee P P, Willisa B C, Moss R L, Jalifea J, Valdivia H H (2015). Arrhythmogenesis in a catecholaminergic polymorphic ventricular tachycardia mutation that depresses ryanodine receptor function. *Proc Natl Acad Sci U S A*. 112(13):E1669-77.
- 1323 25. Dubey GP, Ben-Yehuda S (2011) Intercellular nanotubes mediate bacterial communication. *Cell* 144(4):590-600.
- 1324 26. Rustom A, Saffrich R, Markovic I, Walther P, Gerdes HH (2004) Nanotubular highways for intercellular organelle transport. *Science* 303(5660):1007-1010.
- 1325 27. Franzini-Armstrong C. (2007) ER-Mitochondria Communication. How Privileged? *Physiol-ogy* 22:261-268.
- 1326 28. Lavorato L, Huang TQ, Iyer VR, Perni S, Meissner G, Franzini-Armstrong C (2015). Dyad content is reduced in cardiac myocytes of mice with impaired calmodulin regulation of RyR2. *J Muscle Res Cell Motil*. 36(2):205-14.
- 1327 29. Franzini-Armstrong, Boncompagni S (2011) The Evolution of the Mitochondria-to-Calcium Release Units Relationship in Vertebrate Skeletal Muscles. *J Biomed Biotechnol*, vol. 2011, Article ID 830573. doi:10.1155/2011/830573.
- 1328 30. Yuen B, Boncompagni S, Feng W, Yang T, Lopez J R, Matthaeci K I, Goth SR, Protasi F, Franzini-Armstrong, C, Allen P, Pessah I N (2012) Mice expressing T4826I-RYR1 are viable but exhibit sex- and genotype-dependent susceptibility to malignant hyperthermia and muscle damage. *FASEB J* 26: 1311-1322, 2012.
- 1329 31. Dorn G (2012). Mitochondrial dynamics in heart disease. *Biochim Biophys Acta Mol* 1833(1): 233-241.